Motion of packings of frictional grains

Thomas C. Halsey*
ExxonMobil Upstream Research Co., 3120 Buffalo Speedway, Houston, Texas 77098, USA
(Received 11 March 2009; published 6 July 2009)

Friction plays a key role in controlling the rheology of dense granular flows. Counting the number of constraints vs the number of variables indicates that critical coordination numbers $Z_c=3$ (in $D=2$) and $Z_c=4$ (in $D=3$) are special, in that states in which all contacts roll without frictional sliding are naively possible at and below these average coordination numbers. We construct an explicit example of such a state in $D=2$ based on a honeycomb lattice. This state has surprisingly large values for the typical angular velocities of the particles. Solving for the forces in such a state, we conclude that organized shear can exist in this state only on scales $\ell < d/I$, where d is the grain diameter and $I=d\dot{\gamma}/\sqrt{P/\rho_g}$ is the dimensionless "inertia number." Above this scale the coherent shear is destabilized by the disappearance of normal forces between a significant fraction of the grains. Moving to disordered lattices, we observe that rolling regions in such lattices are characterized by an antiferromagnetic short-range ordering of the particle rotations; the frustration of this ordering links the shearing states of the grain packing to low-energy spin-glass states on the same lattice. Random lattice states are also expected to exhibit large values for the typical angular velocities and to also have regions of coherent shear limited to be smaller than ℓ.

DOI: 10.1103/PhysRevE.80.011303 PACS number(s): 45.70.−n, 81.05.Rm, 75.10.Nr

I. INTRODUCTION

Flows of hard granular systems are ubiquitous in nature and technology, yet are still poorly understood. Compared to truly microscopic dynamical or statistical mechanical systems, an unusual feature of granular systems is that they are intrinsically frictional and dissipative. Not only can dissipation arise through inelastic collisions between the particles, but also from frictional sliding between smooth or rough grain surfaces.

In the quasistatic "critical state" regime [1], the strain rates are smaller than any time scale of the system. In this regime, there are clearly particle contacts whose lifetime is comparable to an inverse strain rate $\dot{\gamma}^{-1}$. Over the past few years, it has become increasingly evident that long-lived contacts are also a feature of the "dense granular flow" regime, marked by strain rates obeying

$$\sqrt{P/\rho_g L^2} < \dot{\gamma} < \sqrt{P/\rho_g d^2}, \tag{1}$$

with P as the pressure, ρ_g the density, L a characteristic flow scale, and d the grain diameter. These features distinguish these regimes from a higher strain-rate regime dominated by two-particle collisions, which has been the object of kinetic-theory based studies [2].

The degree to which such studies can be extended into the dense granular flow regime defined by Eq. (1) remains controversial. A number of authors have claimed that key aspects of the rheology of dense granular flow can be recovered within kinetic-theory treatments that include particle inelasticity and interparticle friction [3]. Halsey and Ertaş [4], and Jenkins [5], have posited the appearance of coherent structures in dense granular flows, which are difficult to reconcile with the underlying assumptions of kinetic theories. A significant work by the group author GDR Midi [6] pointed out that much of the phenomenology of dense granular flows can be organized using the "inertia number"

$$I \equiv d\dot{\gamma}/\sqrt{P/\rho_g}. \tag{2}$$

An interesting feature of these results is the anomalously large fluctuations in the grain velocities, which scale with I in the dense flow regime,

$$\frac{\langle(\vec{v}(\vec{x}) - \langle\vec{v}(\vec{x})\rangle)^2\rangle}{(\dot{\gamma}d)^2} \sim I^{-\chi}, \tag{3}$$

where in dimensionalities $D=2,3$, $\chi \approx 1$ [6,7].

Setting

$$I \equiv d/\ell, \tag{4}$$

defines the scale ℓ of the coherent structures hypothesized by Halsey and Ertaş, which account for the overall structure of the "phase diagram" for incline flow, but whose microscopic meaning is still elusive [4,8,9].

In this work I turn to the role of friction at enduring contacts in these flows. Provided that the microscopic coefficient of friction μ defining the maximum value of the tangential force T at a contact divided by the normal force N is appreciable, we would anticipate that a significant fraction of long-lived contacts in a flowing granular packing will be rolling as opposed to sliding.

Simple counting of the number of constraints vs the number of variables indicates that states in which all contacts are rolling are not possible at coordination numbers $Z_c > 3$ for $D=2$ or $Z_c > 4$ for $D=4$. These results are simple extensions to the dynamical case of the famous "isostatic" criteria for static packings [10].

An interesting soluble case in $D=2$ is presented by the honeycomb lattice, for which all particles have a coordination number $Z_c=3$ exactly. This allows for a general solution of all states obeying the rolling constraint, corresponding to a full solution of the kinematics for this packing, in the limit

*thomas.c.halsey@exxonmobil.com

$\mu \to \infty$, over times short enough that collisions do not degrade the lattice. It is also possible to solve exactly for the both the tangential and normal forces exerted between the particles in this lattice; I present this explicitly for a particularly symmetric case of motion.

A striking feature of the kinematic solution is that even if the overall shear remains moderate, the rotational velocities of the particles are quite large. For a region of the packing of size ℓ with a constant shear $\dot{\gamma}$, the typical rotational velocity of the particles is $\omega \sim \dot{\gamma}\ell/d$. Corresponding to these enhanced rotations, forces develop that limit the size of these regions of constant shear to

$$\ell < \frac{\sqrt{P/\rho_g}}{\dot{\gamma}}, \tag{5}$$

due to the requirement that all normal forces remain compressive. (Dry granular packings are unable to support tensions between the particles.) Equation (5) corresponds to the definition of the coherent structure size ℓ given in Eqs. (2) and (4) above.

Turning to disordered lattices, we see that the rotations arise from an underlying short-ranged antiferromagnetic ordering in the rotational velocities of the individual grains. This short-ranged ordering is frustrated by the existence in disordered lattices of "odd plaquettes" with odd numbers of links around the plaquette. In fact, it follows that it is not possible, even for quite large values of the coefficient of friction, for all of the particle contacts in a lattice with odd plaquettes to be rolling contacts. However, if sliding contacts are allowed, such that every odd plaquette has at least one sliding contact, then the remaining contacts can be rolling contacts; results on spin glasses then imply that it is possible that long-range-ordered antiferromagnetic "spin-glass" regions will form. Of course, given the lack of direct correspondence between a statistical mechanical model (spin glasses) and a driven dissipative nonequilibrium system, it is not possible to draw rigorous conclusions from this analogy.

The remainder of this paper is divided into four sections. In Sec. II, we derive the critical coordination numbers for rolling states and we solve the rolling kinematics of the honeycomb lattice. In Sec. III, we solve a special case for the dynamics of this state. In Sec. IV, we turn to disordered lattices in $D=2$, using a Fokker-Planck approach to show the basis for the antiferromagnetic ordering and the analogy to spin glasses. We also comment on the applicability of these results to the three-dimensional case. In Sec. V, we conclude.

II. KINEMATICS OF ROLLING STATES

Consider a set of N_g spherical grains of diameter d, indexed by i, in D dimensions with velocities $\vec{v}_i$ and rotational velocities (in $D=2$ or $D=3$, the generalization to higher dimensions is obvious) $\vec{\omega}_i$. We further suppose the existence of pairs of grains $\langle ij \rangle$ in contact with one another, and for which there is no relative motion of the surface points in contact (corresponding to frictional locking of the particles.) Suppose that the vector connecting the pair $\langle ij \rangle$ is $\delta\vec{w}_{\langle ij \rangle}$, with $|\delta\vec{w}_{\langle ij \rangle}| = d$. Then the requirement that the relative motion of the surface points in contact be zero is

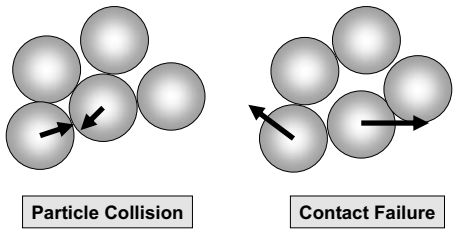

FIG. 1. Two types of crisis can disrupt a lattice of rolling grains: (a) two grains collide creating a new contact or (b) two grains separate due to the normal force between them reaching zero.

$$\vec{v}_i - \vec{v}_j \equiv \delta\vec{v}_{\langle ij \rangle} = \frac{1}{2}(\vec{\omega}_i + \vec{\omega}_j) \times \delta\vec{w}_{\langle ij \rangle}. \tag{6}$$

Taking the derivative with respect to time of this constraint yields a constraint for the accelerations of the grains $\vec{a}_i$ and angular accelerations $\vec{\Gamma}_i$,

$$\delta\vec{a}_{\langle ij \rangle} = \frac{1}{2}(\vec{\omega}_i + \vec{\omega}_j) \times \delta\vec{v}_{\langle ij \rangle} + \frac{1}{2}(\vec{\Gamma}_i + \vec{\Gamma}_j) \times \delta\vec{w}_{\langle ij \rangle}. \tag{7}$$

These equations substantially constrain both the motion of the grains and the forces between the grains. Equation (6) gives $D-1$ constraints per contact. The requirement that the grains stay in contact gives one further constraint. Since each particle has $D(D+1)/2$ degrees of freedom without contacts, this means that the total number of degrees of freedom N_F is

$$\frac{N_F}{N_g} = \frac{D}{2}(D + 1 - Z_c), \tag{8}$$

where Z_c is the average coordination number of the grains. We thus see that the average coordination $Z_c \leq D+1$ in order for the rolling state to be mobile at all, and Eq. (8) then gives the effective number of degrees of freedom remaining to the packing.

The forces are even more completely determined. The total number of contact forces is exactly the same as the number of constraints on the accelerations given by Eq. (7), with the result that all of these forces are determined by the contact network, the velocities and angular velocities of the particles, and the boundary conditions, even for $Z_c < D+1$. (This result can be extended to the case of sliding contacts [11].)

With the kinematics thus determined, the equations of motion of the particles can be integrated forward, until one of two possible types of crisis occurs to disrupt the network (see Fig. 1).

(1) If two grains collide, they will very rapidly (within a collision time set by the Young's modulus of the particles) establish a contact with a finite normal force. This also changes the network, and hence the kinematics. In this case the impulse arising from the collision will, in general, result in a jump in the velocities and forces, which may be significant in the neighborhood of the new contact. Corresponding to the change in kinetic energy caused by the velocity jumps there will be a net energy dissipation because of the collision event [12].

(2) If the normal force between two grains becomes zero, the grains will separate. This effectively changes the contact

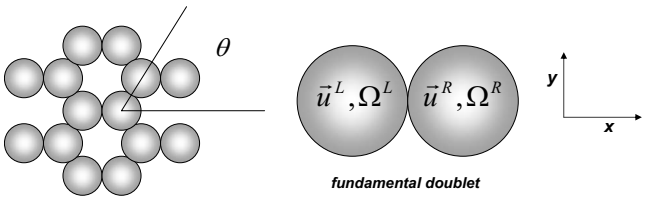

FIG. 2. A honeycomb lattice has the critical coordination number $Z_c=3$ at which a frictional packing becomes mobile in $D=2$. We work with a set of honeycomb lattices characterized by the single parameter θ. We also show the fundamental "doublet" and the coordinate system.

network and the kinematics must now be solved with the new contact network. However, we do not anticipate that this change in kinematics will correspond to any jump in the velocities or forces. This event does not lead to any dissipation. In a statistical steady state, the number of contact failures per unit time should equal the number of new contacts created by collisions per unit time.

A. Honeycomb lattice

In $D=2$, we can construct an explicit example of a rolling state at the critical coordination number $Z_c=3$ by considering a honeycomb lattice (Fig. 2). We consider a relatively symmetric lattice, characterized by one angle θ; the basic plaquettes of the lattice are equilateral (although not necessarily regular) hexagons.

We describe the system as a lattice of "doublets" made up of two grains in contact. The positions of these doublets we index by (j,k), with either j,k both even, or j,k both odd. The positions of the centers of the doublets are then $(x,y)=(c_x j, c_y k)$, with $c_x=d(1+\cos\theta)$ and $c_y=d\sin\theta$. Note that the axes of the Bravais lattice of doublets are oriented along the angles $\pm\theta/2$. With the doublets oriented along the x axis, the requirement that the two grains stay in contact and have a rolling contact constrains the velocities and rotational velocities of the left-hand and right-hand grains, $u_x^L,u_y^L,\Omega^L;u_x^R,u_y^R,\Omega^R$,

$$u_x^L=u_x^R\equiv u_x,\quad u_y^L\equiv u_y-\frac{d}{4}(\Omega^L+\Omega^R),\tag{9}$$

$$u_y^R\equiv u_y+\frac{d}{4}(\Omega^L+\Omega^R),$$

which reduces the 6 degrees of freedom of the two grains taken independently to the 4 degrees of freedom remaining after the imposition of the constraint that the contact be a permanent rolling contact. These 4 degrees of freedom are conveniently taken as the average x and y velocities of the doublet, u_x, u_y, and two (redimensioned) combinations of the two rotational velocities $\Delta=\frac{d}{2}(\Omega^L+\Omega^R)$, $\xi=\frac{d}{2}(\Omega^L-\Omega^R)$.

Now let us consider the constraints imposed by the requirement that the contacts between the doublet and other grains be rolling. Consider the contacts between the doublet at j,k and the doublets at $j-1,k-1$ and $j+1,k-1$. Let us write the vector $z(j,k)$ describing the doublet kinematical state,

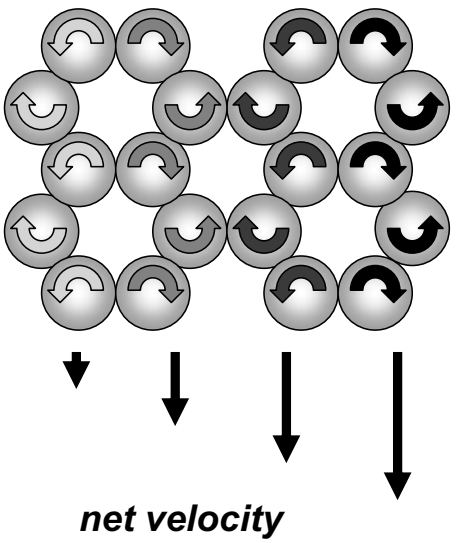

FIG. 3. The β_2 mode from Eq. (22) corresponds to grains counter-rotating in each vertical chain, with the magnitude of the rotations increasing linearly with the coordinate x. This generates an overall pure shear with the velocity in the vertical direction.

$$z(j,k)=[u_x(j,k),u_y(j,k),\Delta(j,k),\xi(j,k)].\tag{10}$$

In Appendix A, we determine the contact rolling equations as having the hyperbolic form

$$z(j,k)=\bar{A}_-z(j-1,k-1)+\bar{A}_+z(j+1,k-1),\tag{11}$$

with $\bar{A}_-(\theta)$ and $\bar{A}_+(\theta)$ given by Eqs. (A4) and (A5).

Solutions to this equation can be written in the Bloch-Floquet form

$$z(j,k)=\int_{-\pi/2}^{\pi/2}\frac{dq}{\pi}e^{\imath qj}\sum_{n=1}^{4}\alpha_n(q)[\lambda_n(q)]^k v_n(q),\tag{12}$$

with

$$\bar{A}(q)v_n(q)=\lambda_n(q)v_n(q),\tag{13}$$

where $\bar{A}(q)$ is determined from Eqs. (A4) and (A5),

$$\bar{A}(q)=\cos(q)\begin{pmatrix}1&0&0&0\\0&1&0&0\\0&0&-1&0\\0&0&0&1\end{pmatrix}+\imath\sin(q)\times\begin{pmatrix}0&-\tan\left(\frac{\theta}{2}\right)&0&-\frac{1}{2}\tan\left(\frac{\theta}{2}\right)\\-\cot(\theta)&0&-\frac{1}{2}&0\\0&\frac{2}{1+\cos\theta}&-1&-\frac{\cos\theta}{1+\cos\theta}\\-2\csc\theta&0&1&0\end{pmatrix}.\tag{14}$$

We can now directly diagonalize $\bar{A}(q)$ to obtain the eigenvalues and eigenvectors:

$$\{\lambda_1(q);v_1\} = \{-1;[0,-1/2,\imath\cot(q/2),1]\}, \tag{15}$$

$$\{\lambda_2(q);v_2\} = \{1;[0,-1/2,-\imath\tan(q/2),1]\}, \tag{16}$$

$$\{\lambda_3(q);v_3\} = \left\{e^{-\imath q};\left[\frac{\sin\theta}{2},\frac{\cos\theta}{2},0,1\right]\right\}, \tag{17}$$

$$\{\lambda_4(q);v_4\} = \left\{e^{\imath q};\left[-\frac{\sin\theta}{2},\frac{\cos\theta}{2},0,1\right]\right\}. \tag{18}$$

These modes can obviously be combined to give a wide variety of different possible motions. We are most interested, however, in motions corresponding to low wave number deformations of the lattice. We thus consider $q \ll 1$, and we expand the integrand from Eq. (12), taking only one wave vector for convenience,

$$\sum_{n=1}^{4}\alpha_n(q)[\lambda_n(q)]^k \exp(\imath qj)v_n \approx \alpha_1(q)(-1)^k(1+\imath qj) + \alpha_2(q)(1+\imath qj)\begin{pmatrix}0\\-1/2\\\imath\tan(q/2)\\1\end{pmatrix} + \alpha_3(q)(1+\imath q(j-k))\begin{pmatrix}\frac{\sin\theta}{2}\\\frac{\cos\theta}{2}\\0\\1\end{pmatrix} + \alpha_4(q)(1+\imath q(j+k)\}\begin{pmatrix}\frac{\sin\theta}{2}\\\frac{\cos\theta}{2}\\0\\1\end{pmatrix} + O(q^2). \tag{19}$$

To this, we can clearly add constant values of u_x, u_y, and Δ. We can also add a constant value of $\xi = \Omega^L - \Omega^R$, since in a honeycomb lattice we can always set alternate grains rotating in opposite directions with the same angular velocity without creating any large-scale motion. We thus collect only those terms that depend on j,k. For convenience, we also define

$$\beta_1 = -2\alpha_1, \tag{20}$$

$$\beta_{2,3,4} = \imath\alpha_{2,3,4}q, \tag{21}$$

with $\beta \in \Re$, so that taking the limit $q \to 0$ and taking the real part, we obtain the general solution (for constant velocity gradients)

$$z(j,k) = \begin{Bmatrix} \frac{\sin(\theta)}{2}[\beta_3(j-k) - \beta_4(j+k)] \\ \frac{\cos(\theta)}{2}[\beta_3(j-k) + \beta_4(j+k)] - \frac{\beta_2}{2}j + \frac{\beta_1}{4}(-1)^k \\ \beta_1 j(-1)^k \\ \beta_2 j + \beta_3(j-k) + \beta_4(j+k) - \frac{\beta_1}{2}(-1)^k \end{Bmatrix}. \tag{22}$$

Note that for $\beta_1 \neq 0$, but $\beta_{2,3,4} = 0$, there is no large-scale motion of the lattice, but rather compensating motions of neighboring doublets. Although we have not introduced the concept of an excitation energy, the β_1 mode is reminiscent of "optical" modes in standard lattice dynamics, which have finite energy even at zero wave vector, and correspond similarly to compensating motions inside a Bravais lattice cell.

The other three "acoustic" modes correspond to simple shear motions. The β_2 mode corresponds to shear along the y direction (Fig. 3), while the β_3 and β_4 modes correspond to flow perpendicular to the directions $\pm\theta$ (see Fig. 4). Flows such as extensional flows that combine simple shear motions can be easily constructed from these three simple shearing modes.

It is notable that in all of the simple shearing modes, the parameter $\xi = \Omega^L - \Omega^R$ increases linearly across the shearing region (Fig. 3). While the average angular velocity $\langle\omega\rangle$ obeys

$$\langle\omega\rangle \sim \dot{\gamma}, \tag{23}$$

where $\dot{\gamma}$ is the overall shear, the average value of the angular velocity squared, $\langle\omega^2\rangle$ depends additionally on the size of the system (or of the coherently shearing region within the system) ℓ,

$$\langle\omega^2\rangle \sim \left(\frac{\dot{\gamma}\ell}{d}\right)^2. \tag{24}$$

III. FORCES IN ROLLING STATES

Simply showing that a state is kinematically possible does not imply that it is dynamically feasible—to accomplish the latter, we must also determine a set of interparticle forces with which it is consistent. For a granular system, this will be a set of normal forces N and tangential forces T across each contact, subject to the two constraints that $N > 0$, since grains

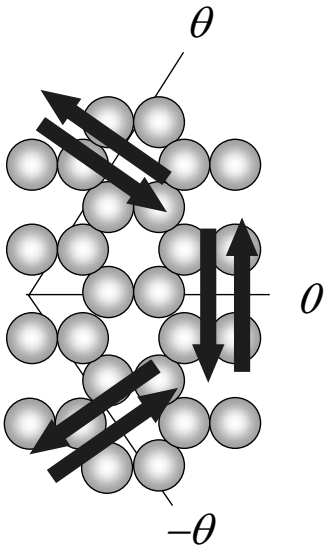

FIG. 4. The three acoustic modes of the kinematics correspond to shear directed perpendicular to the y axis and perpendicular to the directions $\pm\theta/2$.

cannot exert tensional forces on one another, and $T \leq \mu N$, with μ as the coefficient of friction.

Considering a doublet at position (j,k), we see that such a doublet is influenced by eight forces exerted across its four contacts, as well as by two internal forces exerted by the two grains on one another. It is convenient to use a geographical notation to describe the external forces—the forces exerted by the doublet at $(j-1,k+1)$ on the doublet at (j,k) are termed N_{NW}, T_{NW}, with T defined so that a force in the counterclockwise direction is positive. Similarly, we define the forces exerted by the $(j+1,k+1)$, $(j+1,k-1)$ and $(j-1,k-1)$ doublets, respectively, as (N_{NE},T_{NE}), (N_{SE},T_{SE}), and (N_{SW},T_{SW}) (see Fig. 5). The force exerted at the internal contact is (N_0,T_0), with T_0 defined so that $T_0>0$ corresponds to a counterclockwise force on each grain.

With some tedious but straightforward algebra, we can convert the six equations of motion of the two particles in the doublet into four equations coupled to our natural kinematical variables, plus two equations determining the internal

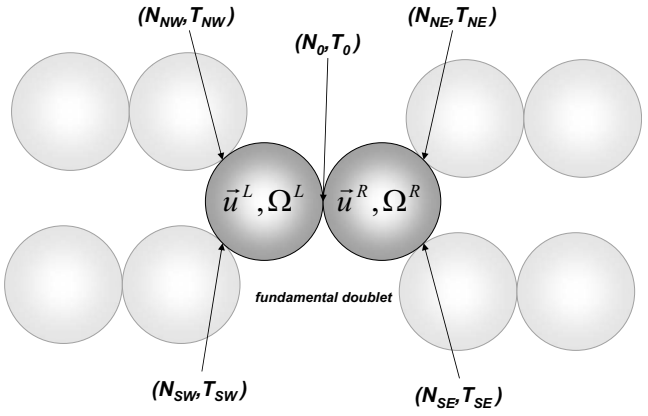

FIG. 5. Eight forces are exerted on a fundamental doublet of the honeycomb lattice by its neighbors; two additional forces are exerted by the doublet particles on one another.

forces N_0, T_0. We write M and I_M for the masses and moments of inertia of the grains, with $\kappa = I_M/Md^2$. Details of the computation are given in Appendix B. The result for the dynamical equation for the doublet is

$$\begin{pmatrix} N_{NW} \\ T_{NW} \\ N_{NE} \\ T_{NE} \end{pmatrix} = \bar{B}(\theta) \begin{pmatrix} N_{SW} \\ T_{SW} \\ N_{SE} \\ T_{SE} \end{pmatrix} + 2M\bar{C}(\theta) \begin{pmatrix} \dot{u}_x \\ \dot{u}_y \\ (1+\kappa)\dot{\Delta} \\ \kappa\dot{\xi} \end{pmatrix}, \quad (25)$$

with $\bar{B}(\theta)$ and $\bar{C}(\theta)$ given by Eqs. (B11) and (B12).

Note that $[N_{SW}(j,k),T_{SW}(j,k)]=[N_{NE}(j-1,k-1),T_{NE}(j-1,k-1)]$, with equivalent identities for the other forces. The forces can be written as

$$\begin{pmatrix} N_{NW}(j,k) \\ T_{NW}(j,k) \\ N_{NE}(j,k) \\ T_{NE}(j,k) \end{pmatrix} = \int_{-\pi/2}^{\pi/2} \frac{dq}{\pi} e^{iqj} \begin{pmatrix} N_{NW}(q,k) \\ T_{NW}(q,k) \\ N_{NE}(q,k) \\ T_{NE}(q,k) \end{pmatrix}. \quad (26)$$

We then can immediately write the equation determining solutions to the homogeneous problem,

$$\begin{pmatrix} N_{NW}(q,k) \\ T_{NW}(q,k) \\ N_{NE}(q,k) \\ T_{NE}(q,k) \end{pmatrix} = \bar{B}(\theta)\bar{D}(q) \begin{pmatrix} N_{NW}(q,k-1) \\ T_{NW}(q,k-1) \\ N_{NE}(q,k-1) \\ T_{NE}(q,k-1) \end{pmatrix}, \quad (27)$$

with

$$\bar{D}(q) = \begin{pmatrix} 0 & 0 & e^{-iq} & 0 \\ 0 & 0 & 0 & e^{-iq} \\ e^{iq} & 0 & 0 & 0 \\ 0 & e^{iq} & 0 & 0 \end{pmatrix}. \quad (28)$$

The eigenvalues and eigenvectors $\{\nu_n;u_n\}$ of $\bar{\mathcal{B}}(\theta,q) = \bar{B}(\theta)\bar{D}(q)$ are given by

$$\{\nu_1(q);u_1\} = \{-1;[e^{-iq}\tan\theta, e^{-iq}, -\tan\theta, 1]\}, \quad (29)$$

$$\{\nu_2(q);u_2\} = \{1;[-e^{-iq}\tan\theta, -e^{-iq}, -\tan\theta, 1]\}, \quad (30)$$

$$\{\nu_3(q);u_3\} = \{e^{-iq};[0,0,\cot(\theta/2),1]\}, \quad (31)$$

$$\{\nu_4(q);u_4\} = \{e^{iq};[-\cot(\theta/2),1,0,0]\}. \quad (32)$$

These eigenvectors are in fact quite intuitive. Each of the eigenvectors 2–4 corresponds to a set of parallel force chains in one direction in the lattice, as is illustrated in Fig. 6; eigenvector 1 is more complex.

Given the homogeneous solutions, it is straightforward to determine the solution to the inhomogeneous problem for which the packing is moving. Writing

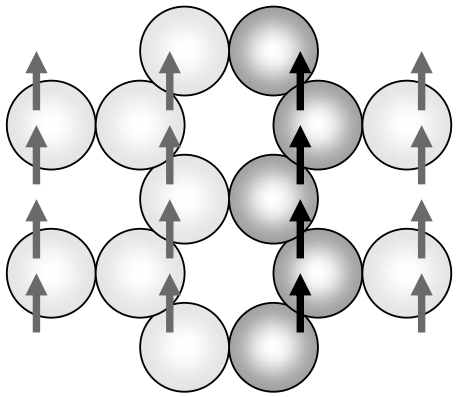

FIG. 6. The fundamental homogeneous modes of the forces correspond principally to force chains, including both normal and tangential forces, directed along the lattice directions of the honeycomb lattice. The force chains shown correspond to the second force eigenvector given in Eq. (30).

$$2M\bar{C}(\theta)\begin{pmatrix} \dot{u}_x(q,k) \\ \dot{u}_y(q,k) \\ (1+\kappa)\dot{\Delta}(q,k) \\ \kappa\dot{\xi}(q,k) \end{pmatrix} = \sum_{n=1}^{4} \upsilon_n(q,k)u_n(\theta,q), \quad (33)$$

with

$$\upsilon_n(j,k) = \int_{-\pi/2}^{\pi/2} \frac{dq}{\pi} e^{iqj}\upsilon_n(q,k), \quad (34)$$

we have the inhomogeneous equation

$$\begin{pmatrix} N_{NW}(q,k) \\ T_{NW}(q,k) \\ N_{NE}(q,k) \\ T_{NE}(q,k) \end{pmatrix} = \bar{\mathcal{B}}(\theta,q)\begin{pmatrix} N_{NW}(q,k-1) \\ T_{NW}(q,k-1) \\ N_{NE}(q,k-1) \\ T_{NE}(q,k-1) \end{pmatrix} + \sum_{n=1}^{4} \upsilon_n(q,k)u_n. \quad (35)$$

This equation is easy to solve. Writing

$$\begin{pmatrix} N_{NW}(q,0) \\ T_{NW}(q,0) \\ N_{NE}(q,0) \\ T_{NE}(q,0) \end{pmatrix} = \sum_{n=1}^{4} \tau_n(q)u_n, \quad (36)$$

we immediately obtain

$$\begin{pmatrix} N_{NW}(q,k) \\ T_{NW}(q,k) \\ N_{NE}(q,k) \\ T_{NE}(q,k) \end{pmatrix} = \sum_{n=1}^{4} \left[\sum_{k'=0}^{k-1} \nu_n^{k'}\upsilon_n(q,k-k') + \nu_n^k\tau_n(q) \right] u_n. \quad (37)$$

As an example, let us consider extensional flow: $u_x \propto x$, $u_y \propto -y$. This type of flow has the advantage that it preserves the overall symmetries of the honeycomb lattice, and can thus be interpreted parametrically by making the angle θ a function of time, $\theta(t)$. Let us choose the simple case that

$$\theta(t) = -\Lambda t + \theta_0, \quad (38)$$

with $\Lambda > 0$.

We now use Eq. (22) to write a standard form for the velocities $z(j,k)$,

$$z(j,k) = \alpha e^{\iota qj}\left[e^{\iota qk}\begin{pmatrix} -\frac{\sin\theta}{2} \\ \frac{\cos\theta}{2} \\ 0 \\ 1 \end{pmatrix} - e^{-\iota qk}\begin{pmatrix} \frac{\sin\theta}{2} \\ \frac{\cos\theta}{2} \\ 0 \\ 1 \end{pmatrix} \right]. \quad (39)$$

To recover the desired extensional flow, we set $\alpha \equiv -\Lambda d/2\iota q$, take the real part, and take the limit $q \to 0$,

$$z(j,k) = \mathrm{Re}\left\{ \lim_{q\to 0} \frac{-d\Lambda e^{\iota qj}}{2\iota q}\begin{pmatrix} -\cos(qk)\sin\theta \\ \iota\sin(qk)\cos\theta \\ 0 \\ 2\iota\sin(qk) \end{pmatrix} \right\} = \frac{d\Lambda}{2}\begin{pmatrix} j\sin\theta \\ -k\cos\theta \\ 0 \\ -2k \end{pmatrix}. \quad (40)$$

Note that we have chosen α to set the value of $\Delta(j,k)$ to be consistent with Eq. (38). (Note that for a system of extensions parallel to x and y respectively of L_x and L_y, the instantaneous Poisson's ratio $-(L_x/L_y)(\dot{L}_y/\dot{L}_x) = \cot\theta$.) We can now also write the acceleration vector as a limit,

$$\dot{z}(j,k) = \mathrm{Re}\left\{ \lim_{q\to 0} \frac{d\Lambda^2 e^{\iota qj}}{2\iota q}\begin{pmatrix} -\cos(qk)\cos\theta \\ -\iota\sin(qk)\sin\theta \\ 0 \\ 0 \end{pmatrix} \right\} = -\frac{d\Lambda^2}{2}\begin{pmatrix} j\cos\theta \\ k\sin\theta \\ 0 \\ 0 \end{pmatrix}. \quad (41)$$

Note that the accelerations are approximately directed toward the origin and are independent of the sign of Λ, as we would expect for grains engaged in radial motion about one another. We can now use this result to compute the $\{\upsilon\}$ and insert in Eq. (37) to obtain the forces. For the moment we restrain ourselves from taking the limit $q \to 0$, although we do omit some terms that will disappear in this limit, and we obtain

$$\begin{pmatrix} v_1(q,k) \\ v_3(q,k) \\ v_3(q,k) \\ v_4(q,k) \end{pmatrix} \approx -\frac{dM\Lambda^2[\cos\theta\tan(\theta/2)]}{2\imath q}\begin{pmatrix} 0 \\ \imath qk \\ -e^{\imath qk} \\ -e^{-\imath qk} \end{pmatrix}, \tag{42}$$

from which the inhomogeneous contribution to the forces from Eq. (37) can be easily determined, using the limiting expression

$$\begin{pmatrix} N_{NW}(j,k) \\ T_{NW}(j,k) \\ N_{NE}(j,k) \\ T_{NE}(j,k) \end{pmatrix}_{inhom.} = \mathrm{Re}\left\{ \lim_{q\to 0} e^{iqj} \sum_{n=1}^{4} \left[\sum_{k'=0}^{k-1} \nu_n^{k'} v_n(q,k-k') \right] u_n \right\}, \tag{43}$$

$$\begin{pmatrix} N_{NW}(j,k) \\ T_{NW}(j,k) \\ N_{NE}(j,k) \\ T_{NE}(j,k) \end{pmatrix}_{inhom.} = \frac{dM\Lambda^2}{2}[\cos\theta\tan(\theta/2)]\left\{ \frac{k^2}{2}\begin{pmatrix} \tan\theta \\ 1 \\ \tan\theta \\ -1 \end{pmatrix} + jk\begin{pmatrix} -\cot(\theta/2) \\ 1 \\ \cot(\theta/2) \\ 1 \end{pmatrix} \right\}. \tag{44}$$

where we have neglected terms of less than quadratic order in j,k.

It is clear that this inhomogeneous contribution includes negative values of the normal forces at sufficiently low values of k/j, and that these scale with k^2 (at fixed k/j). In addition, it is now easy to determine the inhomogeneous part of the internal normal force within a doublet, $N_{0,inhom.}$, using Eq. (B5), which yields (at quadratic order in j,k)

$$N_{0,inhom.} = -\frac{dM\Lambda^2 \sin\theta}{2}k^2, \tag{45}$$

which is also negative, and also scales with k^2.

Thus, no matter what the value of the homogeneous term for the forces [corresponding to the term proportional to τ in Eq. (37)], the requirement that normal forces be positive will ultimately be overwhelmed by the growth of the inhomogeneous term. Note that it is the contacts most perpendicular to the direction of acceleration that are most at risk of losing their normal forces. In addition, with a finite coefficient of friction, the tangential forces will ultimately saturate the Coulomb criterion and slippage will occur at grain contacts, invalidating our kinematical assumptions. However, even with an *infinite* coefficient of friction, the motion of the packing is limited to a domain size controlled by the requirement that all normal forces be compressional. If the scale of the homogeneous forces is determined by the average pressure in the packing P, then the scale ℓ of this domain size is determined by

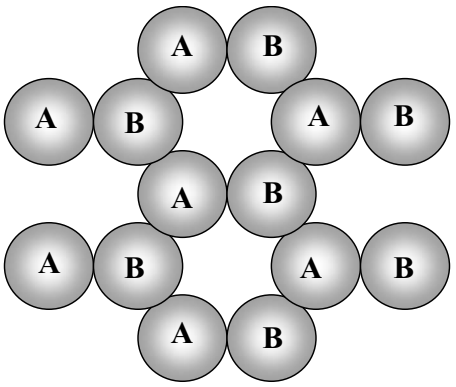

FIG. 7. The honeycomb lattice shear solutions correspond to approximate counter-rotation of two alternating sublattices of grains, here indexed by A and B.

$$\frac{\ell}{d} = \frac{1}{\Lambda d}\sqrt{P/\rho_g}, \tag{46}$$

with the density $\rho_g \sim M/d^2$. Comparing to Eq. (2), we see that this is equivalent to

$$\ell = \frac{d}{I}, \tag{47}$$

which connects the length scale over which frictionally dominated motion can determine the kinematics with the inertia number I, in a manner consistent with the physical picture of Halsey and Ertaş.

Note that this result can also be obtained on dimensional grounds. For a coherently shearing region of size ℓ, the typical angular velocity $\omega \sim \dot{\gamma}\ell/d$ from Eq. (24). Corresponding to this angular velocity, one would anticipate an acceleration at the persistent contacts of

$$\vec{a} \sim \frac{(\dot{\gamma}\ell)^2}{d} \tag{48}$$

which will set a force scale of

$$N \sim M\frac{(\dot{\gamma}\ell)^2}{d}, \tag{49}$$

which is the scale of the inhomogeneous forces computed explicitly above. Note that this suggests that any state in which Eq. (48) holds will also have its regions of coherent shear limited to the scale $\ell = d/I$, including much more disorderly states than the honeycomb lattice. I will return to this point in Sec. IV below.

IV. KINEMATICS OF RANDOM GRAIN PACKINGS

Let us reconsider the kinematics of the honeycomb lattice state, as defined by Eq. (12). An initially surprising feature of this state is the role played by $\xi = \Omega^L - \Omega^R$, which increases linearly with distance in states with overall linear behavior of the average velocities u_x and u_y. Thus, one way to view the motion of the honeycomb state is by decomposing it into alternating sublattices, A and B (see Fig. 7), on which the

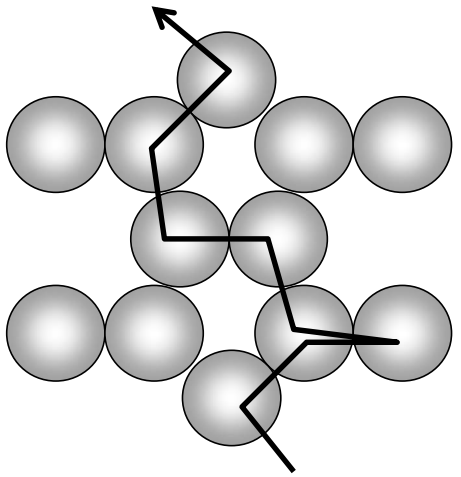

FIG. 8. In the Fokker-Planck approximation, we consider random walks from grain to grain passing always through contacts between the grains.

particles are approximately counter-rotating with respect to one another. The spatial variations of these counter-rotations then determine the overall spatial structure of the flow. Now we must consider random lattices, and determine, in particular, if there is any remnant of this feature for such lattices.

To determine the nature of the random lattice solution that respects the constraining large-scale motions, we apply a two-point Fokker-Planck approximation. Consider a random walk that moves entirely between grains in contact with one another (see Fig. 8). Provided that the instantaneous contact network percolates, such a random walk can access arbitrarily distantly separated parts of the grain packing. Over the set of all particle contacts $\langle ij \rangle$ we can define a probability distribution $\rho(\theta, \delta\vec{v})$ on the angles of the contacts θ_{ij} and the differences in grain velocity across the contacts $\delta\vec{v}_{ij}=\vec{v}_i-\vec{v}_j$. For simplicity of notation we are confining ourselves to two dimensions; however, the generalization to arbitrary dimensions is clear and is assumed in much of the discussion below.

We now assume that in the random walk described in the previous paragraph, subsequent steps in the random walk correspond to uncorrelated choices of $\theta_{ij}, \delta\vec{v}_{ij}$ from the distribution $\rho(\theta, \delta\vec{v})$. (The neglect of correlations in this approximation is clearly dangerous, particularly in lower dimensionalities, of which more later.)

Let us define a matrix corresponding to the average changes in position and velocity corresponding to one step in this random walk,

$$\overline{\mathcal{M}} = \begin{pmatrix} \langle \delta w_x \delta w_x \rangle & \langle \delta w_x \delta w_y \rangle & \langle \delta w_x \delta v_x \rangle & \langle \delta w_x \delta v_y \rangle \\ \langle \delta w_y \delta w_x \rangle & \langle \delta w_y \delta w_y \rangle & \langle \delta w_y \delta v_x \rangle & \langle \delta w_y \delta v_y \rangle \\ \langle \delta v_x \delta w_x \rangle & \langle \delta v_x \delta w_y \rangle & \langle \delta v_x \delta v_x \rangle & \langle \delta v_x \delta v_y \rangle \\ \langle \delta v_y \delta w_x \rangle & \langle \delta v_y \delta w_y \rangle & \langle \delta v_y \delta v_x \rangle & \langle \delta v_y \delta v_y \rangle \end{pmatrix}. \tag{50}$$

In this matrix, the averages are easily written, e.g.,

$$\langle \delta w_x \delta w_x \rangle = \int d\theta \int d(\delta\vec{v}) \rho(\theta, \delta\vec{v}) (d \cos\theta)^2. \tag{51}$$

We can now write directly the limiting result for the probability distribution $\rho_n(\Delta\vec{w}, \Delta\vec{v})$ after n steps of the random walk, with $n \to \infty$,

$$\rho_n(\Delta\vec{w}, \Delta\vec{v}) = \frac{1}{\sqrt{(2\pi n)^4 \det(\overline{\mathcal{M}})}} \times \exp\left\{ -\frac{1}{2n} \left[(\Delta\vec{w} \quad \Delta\vec{v}) \overline{\mathcal{M}}^{-1} \begin{pmatrix} \Delta\vec{w} \\ \Delta\vec{v} \end{pmatrix} \right] \right\}. \tag{52}$$

We can use this probability distribution to compute properties of the velocity distribution arising from the fundamental two-particle correlations expressed in $\overline{\mathcal{M}}$. Thus the expectation value of the velocity at the spatial point $\vec{x}$ is given by

$$\langle \vec{v}(\vec{x}) \rangle = \frac{\int dn \int d\vec{v} (\vec{v}) \rho_n(\vec{x}, \vec{v})}{\int dn \int d\vec{v} \rho_n(\vec{x}, \vec{v})}. \tag{53}$$

As an example, consider a case in which $\langle \delta w_x \delta w_y \rangle = \langle \delta v_x \delta v_y \rangle = 0$, and $\langle \delta w_x \delta v_x \rangle = \langle \delta w_y \delta v_y \rangle = \langle \delta w_y \delta v_x \rangle = 0$, but in which $\langle \delta w_x \delta v_y \rangle \neq 0$. In this case we can write

$$\overline{\mathcal{M}} = \begin{pmatrix} \langle \delta w_x \delta w_x \rangle & 0 & 0 & \langle \delta w_x \delta v_y \rangle \\ 0 & \langle \delta w_y \delta w_y \rangle & 0 & 0 \\ 0 & 0 & \langle \delta v_x \delta v_x \rangle & 0 \\ \langle \delta v_y \delta w_x \rangle & 0 & 0 & \langle \delta v_y \delta v_y \rangle \end{pmatrix}. \tag{54}$$

We can now invert $\mathcal{M}$ and use Eq. (53) to show that

$$\frac{\partial \langle v_y \rangle}{\partial x} = \frac{\langle \delta w_x \delta v_y \rangle}{\langle (\delta w_x)^2 \rangle}, \tag{55}$$

and

$$\frac{\partial \langle v_x \rangle}{\partial x} = \frac{\partial \langle v_{x,y} \rangle}{\partial y} = 0 \tag{56}$$

corresponding to pure shear motion.

In this way, any motion that is linear in the coordinates can be associated with values of the coefficients of the matrix $\overline{\mathcal{M}}$, corresponding to particular correlations of neighboring grains. This approach has an interesting feature; however, in that it leads to divergent fluctuations in dimensions below $D=4$.

The generalization of the above formulae to $\rho_n^{(D)}(\vec{x}, \vec{v})$ with $D>2$ is simple, so we can consider, for instance,

$$\langle (\vec{v}(\vec{x}) - \langle \vec{v}(\vec{x}) \rangle)^2 \rangle = \lim_{N \to \infty} \frac{\int_0^N dn \int d\vec{v} (\vec{v}^2 - \langle \vec{v} \rangle^2) \rho_n^{(D)}(\vec{x}, \vec{v})}{\int_0^N dn \int d\vec{v} \rho_n^{(D)}(\vec{x}, \vec{v})}. \tag{57}$$

Simple power counting leads immediately to the conclusion that

$$\langle(\vec{v}(\vec{x})-\langle\vec{v}(\vec{x})\rangle)^2\rangle \sim N^{2-D/2}. \tag{58}$$

If we suppose that $\ell \sim \sqrt{N}$ corresponds to some maximum "coherent" length scale that can be probed by the random walk, then we see that

$$\langle(\vec{v}(\vec{x})-\langle\vec{v}(\vec{x})\rangle)^2\rangle \sim \ell^{4-D}. \tag{59}$$

Note that assuming that $I=d/\ell$, as is done in the theory of incline flow of Halsey and Ertaş [4], gives a divergence of the squared velocity fluctuation

$$\langle(\vec{v}(\vec{x})-\langle\vec{v}(\vec{x})\rangle)^2\rangle \sim I^{D-4}, \tag{60}$$

compared to the numerical result

$$\langle(\vec{v}(\vec{x})-\langle\vec{v}(\vec{x})\rangle)^2\rangle \sim I^{-\chi}. \tag{61}$$

The numerical results for the values of χ in $D=2,3$ are not definitive on its actual value, although $\chi \approx 1$ in $D=2$ is likely [6], and a similar and perhaps smaller value seems to hold in $D=3$ [7].

It is striking that an argument with so little physics predicts a divergence of the velocity fluctuations with an exponent similar to that observed numerically [6,7]. However, the neglect of correlations undermines the quantitative credibility of this argument [13].

Up to now, we have not implemented any requirement that the velocities be determined by the angular motions of the particles. This is seemingly quite straightforward, e.g., the averages of $\delta\vec{v}$ appearing in $\mathcal{M}$ can easily be written in terms of the angular motions of the particles, using Eq. (6), for the rolling contacts. Then, as remarked above, the percolation of the contact network insures that we can still construct the master probability distribution for the fluctuations of $\Delta\vec{w},\Delta\vec{v}$, as in the above argument. There is, however, a subtle and important flaw in this procedure.

Restricting ourselves for the moment to two dimensions, let us try to determine large-scale variations in the angular velocities Ω_i using a procedure analogous to that we used above for large-scale variations in the velocity. Since the velocity moments for neighboring particles are functions of the sum of the angular velocities, $\vec{v}_i-\vec{v}_j=\hat{z}\times(\vec{w}_i-\vec{w}_j)(\Omega_i+\Omega_j)$, we will restrict ourselves to these variables in computing large-scale variations in Ω, which is feasible provided we consider the combination of two successive steps on the lattice of rolling contacts, as shall be seen below.

If we construct an analogous formula to Eq. (52) for the evolution of the distribution of Ω over a random walk, we can write

$$\frac{\partial\Omega}{\partial x} = \frac{\langle\delta w_x \delta\Omega\rangle}{\langle(\delta w_x)^2\rangle}. \tag{62}$$

Note that we have assumed above that there is a stationary distribution $\rho(\theta,\delta\vec{v}_{ij})$. If such a distribution is not a function of position, then there is no local indicator of position arising either from the angular distribution of contacts, nor from the nearest-neighbor velocity differences. For rolling contacts, this implies, as utilized in the above, a stationary distribution $\rho(\theta,\Omega_i+\Omega_j)$. To use this to evaluate an average of $\Omega_i-\Omega_j$, we can concatenate two subsequent steps in our random walk, from $i\to j\to k$, and write that for this compound step

$$\begin{aligned}\langle\delta w_{x;i\to k}(\Omega_k-\Omega_i)\rangle &= \langle(\delta w_{x;i\to j}+\delta w_{j\to k})\\ &\quad\times[(\Omega_k+\Omega_j)-(\Omega_j+\Omega_i)]\rangle\\ &= d\langle\cos\,\theta_{ij}(\Omega_i+\Omega_j)-\cos\,\theta_{jk}(\Omega_j+\Omega_k)\rangle\\ &= 0,\end{aligned} \tag{63}$$

so that we conclude that it is not possible for a distribution with a stationary $\rho(\theta_{ij},\Omega_i+\Omega_j)$ to describe a grain packing with any large-scale spatial variation in Ω.

However, inspired by the discussion above regarding the role of $\xi=\Omega_A-\Omega_B$ in the honeycomb lattice case, we can immediately construct an exception to this. Suppose the packing of grains connected by rolling contacts can be described as consisting of two disjoint subpackings A and B, so that no two A grains, nor any two B grains, are in rolling contact with one another. In this case, we can posit that the distribution used in the random walk depends on whether one is passing from an A grain to a B grain or vice versa, i.e., $\rho_{AB}(\theta,\Omega_A+\Omega_B)\neq\rho_{BA}(\theta,\Omega_B+\Omega_A)=\rho_{AB}(\theta+\pi,\Omega_A+\Omega_B)$, where this latter requirement follows from the reversibility of the random walk. Then we see that in this case, supposing that i,k are on the A packing, and j is on the B packing,

$$\begin{aligned}\langle\delta w_{x;i\to k}(\Omega_k-\Omega_i)\rangle &= \langle(\delta w_{x;i\to j}+\delta w_{j\to k})[(\Omega_k+\Omega_j)\\ &\quad-(\Omega_j+\Omega_i)]\rangle\\ &= 2d\langle\cos\,\theta_{ij}(\Omega_i+\Omega_j)\rangle_{AB},\end{aligned} \tag{64}$$

where $\langle\,\rangle_{AB}$ is defined as the integral over $\rho_{AB}(\theta,\Omega_A+\Omega_B)$. Now we can develop linear gradients in Ω on sublattice A, provided that the gradient of Ω on the alternating sublattice B has the opposite sign, as in the honeycomb lattice solution.

Thus, the state will be characterized by a function $\Omega_A(x,y)$ on the A sublattice, and by $\Omega_B(x,y)$ on the B sublattice, with

$$\frac{\partial\langle\Omega_A\rangle}{\partial x} \approx -\frac{\partial\langle\Omega_B\rangle}{\partial x} \approx \frac{\langle\cos\,\theta_{ij}(\Omega_i+\Omega_j)\rangle_{AB}}{d\langle(\cos\,\theta_{ij})^2\rangle_{AB}}. \tag{65}$$

This criterion will enforce that relative local particle surface velocities will be small where an A-lattice particle contacts a B-lattice particle, which is suitable to a slowly strained system with frictional contacts. Both Ω_A and Ω_B vary linearly across a shearing region. Thus, the dimensional constraint on the forces, Eq. (49), should still apply for random lattices, resulting in a restriction of the coherently shearing region to a scale $\ell=d/I$. Finally, the overall shear is determined in this case by

$$\frac{\partial\langle v_y\rangle}{\partial w_x} = \frac{\langle\cos^2\,\theta_{ij}(\Omega_i+\Omega_j)\rangle_{AB}}{2d\langle(\cos\,\theta_{ij})^2\rangle_{AB}}. \tag{66}$$

In general, it is not possible to decompose a random lattice into two such sublattices. The situation is analogous to an antiferromagnet on a random graph, for which plaquettes bounded by odd numbers of particles are frustrated; i.e., it is not possible to assign each such particle to a sublattice in such a way that no two particles of the same sublattice are in contact with one another (see Fig. 9) [14]. In order to preserve the structure of the state indicated above, with $\Omega_A\approx-\Omega_B$, we require that enough of the particle contacts are slid-

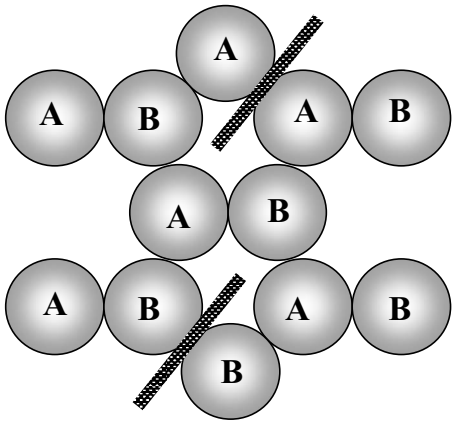

FIG. 9. In a random lattice, a decomposition of the lattice into two alternating sublattices will generally result in "frustrated" contacts, across which sliding must occur.

ing so that all remaining contacts can be rolling contacts between grains on alternate sublattices. It then follows that ρ_{AB} is understood as the distribution across rolling contacts only, not including sliding contacts.

If we wish to apply the reasoning of Eqs. (46)–(49) to the random lattice, and derive a length scale ℓ beyond which a coherently shearing patch will be destabilized by the disappearance of normal forces, we must specify what we mean by a "coherently shearing patch" in a random lattice. For a general random lattice with some density of "odd" plaquettes, there will be a number of possible choices of which contacts must slide so that the others may roll. From the argument of the preceding paragraph, it is clear that this enumeration problem is exactly analogous to the enumeration of the states of an antiferromagnet on the corresponding random graph. The statistical mechanics of this latter problem has been studied—in two dimensions, there appears to be a spin-glass phase at zero temperature, which does not extend to finite temperature [15]. Although the granular problem is not a thermal statistical mechanical problem, it is natural to identify the coherence that is destroyed by the disappearing normal forces with the zero-temperature spin-glass order of the analogous antiferromagnet. With this interpretation of the meaning of "coherence," we again expect

$$\ell = \frac{d}{I} \tag{67}$$

to set the maximum size of a coherent domain, following the argument of Eqs. (46)–(49). A more dramatic indicator of the existence of the state which we are discussing would be a strong short-ranged antiferromagnetic order corresponding to a predominance of rolling contacts.

The overall picture that we have developed should be compared with recent literature on "rolling bearings" [16], which are three-dimensional frictional bearings made up of particles of differing sizes (but lacking odd plaquettes). We can also contrast our results with numerical simulations reported by Alonso-Marroquín *et al.* [17]. In a two-dimensional shear cell, this group observed that the macroscopic shearing motions of a dense granular packing (simulating fault gouge) decomposed, on smaller scales, into regions of coherent vorticity (which in our notation corresponds to Δ constant, $\xi \approx 0$), regions of "ball-bearing motion" (corresponding to the counter-rotating motion of our two sublattices), and shear zones in which sliding dominated. Due to the predominance of rolling contacts, particularly at high coefficients of friction, the overall macroscopic friction observed in the shear cell was considerably less than the microscopic coefficient of friction. The decomposition of the solution into regions with qualitatively different properties violates the assumption that there is a uniform distribution $\rho(\theta, \delta\vec{v})$, on which our argument above was based.

The first of the Alonso-Marroquín motions, corresponding to large-scale vorticity, was not observed in three-dimensional numerical studies specifically designed to look for velocity correlations in chute flows [7]. Also, at high coefficients of friction, the Alonso-Marroquín kinematics was "earthquakelike," with much of the slip occurring in discontinuous jumps. We might suspect that such discontinuous kinetics, associated with pattern formation, are more characteristic of low values of I (corresponding to $\ell \gg L$, with L an overall flow scale), than they are of the intermediate values of I that have been our concern.

Finally, we are also able to use this picture to speculate on the nature of the $\mu \to \infty$ limit. Consider the tangential and normal forces T_c, N_c at a typical sliding contact, $T_c/N_c = \mu$. These forces will be determined by the overall force balances subject to the motions of the grains, and we expect that both T_c and N_c will be $\sim Pd^{D-1}$. Since these forces have a fixed ratio at the sliding contacts, we see that $\lim_{\mu\to\infty} N_c = 0$, since this will be the solution to the force balances in preference to a case in which $T_c \to \infty$. Thus, in the limit, the sliding contacts will see their normal forces driven to zero; i.e., these contacts will be eliminated as physical contacts. We would thus expect that in the limit $\mu \to \infty$ all of the plaquettes will have even numbers of sides, and the frustration will be eliminated, in any mobile state.

A. Three-dimensional case

The extension of these arguments to three dimensions is straightforward. The original contact-rolling equations [Eqs. (6) and (7)] clearly apply in three dimensions, and the diamond lattice plays the same role in $D=3$ of a potential model system as did the honeycomb lattice in $D=2$. To conserve the labor of the author and the patience of the reader, we are not presenting details of the diamond lattice kinematics in this work; we only wish to point out that the diamond lattice does support alternating A and B sublattices analogously to the honeycomb lattice case, which allows shearing states obeying $\vec{\Omega}_A \approx -\vec{\Omega}_B$ to be constructed.

For random lattices, the arguments of the previous section should hold in three dimensions just as in two dimensions (indeed, they should be more valid, since the upper critical dimension of $D=4$ is closer). Again, the optimal decomposition of the random lattice into two alternating sublattices is analogous to the problem of determining a ground state for an antiferromagnet on a random graph. Again, odd plaquettes must have at least one sliding contact corresponding to a

frustrated bond in the random antiferromagnet. In three dimensions, these odd plaquettes can be viewed as threaded by "odd lines," introduced by Rivier and Duffy [18]. For pure shear, we expect the direction of the typical angular velocity to be perpendicular to the shearing motions, so that the analogy is to an Ising antiferromagnet and not to a Heisenberg antiferromagnet. Note that the degenerate case in which particles rotate about an axis through the contact between the particles is assumed not to play a significant role.

V. CONCLUSIONS

The principal conclusions of this study are as follows:

(1) Frictional packings, dominated by rolling contacts, cannot be mobile above a coordination number $Z_c=3(D=2)$ or $Z_c=4(D=3)$. These thresholds are consistent with those obtained using similar arguments by authors studying the isostaticity of static packings.

(2) The honeycomb lattice in $D=2$ offers a case in which the rolling kinematics can be exactly solved. The most surprising feature of the result is that the scale of the angular velocities ω grows linearly with the size of the system, although the average of the angular velocity is moderated by the fact that the rotations on two alternating sublattices roughly cancel.

(3) The dynamics of the honeycomb lattice can also be solved. The conclusion is that the requirement that all normal forces be compressive can only be satisfied for packings smaller than ℓ, with

$$\ell \sim d/I, \tag{68}$$

where I is the inertia number, given by Eq. (2).

(4) For random lattices, a Fokker-Planck approximation to the kinetics yields the same key result as for the honeycomb lattice, i.e., that the typical angular velocity grows linearly with the size of a coherently rolling region. Again, the average angular velocity is much smaller. The presence of odd plaquettes of particles in contact will require compensating sliding contacts even if the coefficient of friction is large; the statistics of these sliding contacts are analogous to those of frustrated bonds in random antiferromagnets.

Clearly, many aspects of the overall kinetics and dynamics of frictional packings remain unaddressed by this study, notably the computation of forces in a random network, and the corresponding overall rheological response of the packing to applied stresses. To solve this latter problem, it will be necessary to understand how regions of coherent rolling organize themselves with respect to one another—is the system still homogeneous in some sense or will sliding contacts organize themselves into defined shear bands?

ACKNOWLEDGMENTS

I am grateful to D. Ertaş for many stimulating discussions and for sharing a number of results prior to publication. I would also like to thank R. Blumenfeld for bringing the existence of Ref. [14] to my attention.

APPENDIX A: HONEYCOMB KINEMATICS

We wish to determine the kinematic constraints on a doublet imposed by the requirement that its internal contact and all contacts with other doublets be rolling. Recall that the doublet under consideration is indexed by the coordinates (j,k), and that the velocity and angular velocity of the left- and right-hand members of this doublet are $u_x^{L,R}, u_y^{L,R}, \Omega^{L,R}$ respectively. Consider the contact between the left-hand doublet member at j,k and the right-hand doublet at $j-1,k-1$. We indicate the velocity and angular velocity of the particle in the $j-1,k-1$ doublet by (v_x^R, v_y^R, ω^R). Then we can conveniently write the new constraints on the velocities by the matrix equation

$$\begin{pmatrix} \cos\theta & \sin\theta \\ -\sin\theta & \cos\theta \end{pmatrix}\begin{pmatrix} v_x^R \\ v_y^R \end{pmatrix} + \frac{d}{2}\begin{pmatrix} 0 \\ \omega^R \end{pmatrix} = \begin{pmatrix} \cos\theta & \sin\theta \\ -\sin\theta & \cos\theta \end{pmatrix}\begin{pmatrix} u_x^L \\ u_y^L \end{pmatrix} - \frac{d}{2}\begin{pmatrix} 0 \\ \Omega^L \end{pmatrix}. \tag{A1}$$

Applying these equations repeatedly to each doublet, we obtain after some labor an equation linking the kth row in the lattice to the $k-1$'st row. Recalling that $u_x^L=u_x^R\equiv u_x$, $u_y^L=u_y-\frac{d}{4}(\Omega^L+\Omega^R)$, $u_y^R=u_y+\frac{d}{4}(\Omega^L+\Omega^R)$, $\Delta=\frac{d}{2}(\Omega^L+\Omega^R)$, and $\xi=\frac{d}{2}(\Omega^L-\Omega^R)$, and writing the variables characterizing a doublet as

$$z(j,k)=[u_x(j,k),u_y(j,k),\Delta(j,k),\xi(j,k)], \tag{A2}$$

we can write the contact rolling equations as

$$z(j,k)=\bar{A}_-z(j-1,k-1)+\bar{A}_+z(j+1,k-1), \tag{A3}$$

with

$$\bar{A}_-=\begin{pmatrix} \frac{1}{2} & \frac{1}{2}\tan\left(\frac{\theta}{2}\right) & 0 & \frac{1}{4}\tan\left(\frac{\theta}{2}\right) \\ \frac{\cot(\theta)}{2} & \frac{1}{2} & \frac{1}{4} & 0 \\ 0 & -\frac{1}{1+\cos\theta} & -\frac{1}{2} & \frac{1}{2}\frac{\cos\theta}{1+\cos\theta} \\ \csc\theta & 0 & -\frac{1}{2} & \frac{1}{2} \end{pmatrix}, \tag{A4}$$

and

$$\bar{A}_+=\begin{pmatrix} \frac{1}{2} & -\frac{1}{2}\tan\left(\frac{\theta}{2}\right) & 0 & -\frac{1}{4}\tan\left(\frac{\theta}{2}\right) \\ -\frac{\cot(\theta)}{2} & \frac{1}{2} & -\frac{1}{4} & 0 \\ 0 & \frac{1}{1+\cos\theta} & -\frac{1}{2} & -\frac{1}{2}\frac{\cos\theta}{1+\cos\theta} \\ -\csc\theta & 0 & \frac{1}{2} & \frac{1}{2} \end{pmatrix}. \tag{A5}$$

APPENDIX B: HONEYCOMB DYNAMICS

Recalling the doublet experiencing forces from its neighbors as in Fig. 5, we see that four of the equations of motion for this doublet can be written as

$$(N_{NW}+N_{SW}-N_{NE}-N_{SE}) \times\cos\theta+(T_{SW}+T_{SE}-T_{NW}-T_{NE})\sin\theta=2M\dot{u}_x, \tag{B1}$$

$$(N_{SW}+N_{SE}-N_{NW}-N_{NE}) \times\sin\theta+(T_{NE}+T_{SE}-T_{NW}-T_{SW})\cos\theta=2M\dot{u}_y, \tag{B2}$$

$$(N_{NW}+N_{SE}-N_{NE}-N_{SW})\sin\theta+(T_{NE}+T_{SE}+T_{NW}+T_{SW}) \times(1+\cos\theta)=\left(2M+\frac{2I_M}{d^2}\right)\dot{\Delta}, \tag{B3}$$

$$T_{NW}+T_{SW}-T_{NE}-T_{SE}=\frac{2I_M}{d^2}\dot{\xi}. \tag{B4}$$

The other two equations of motion are

$$(N_{NW}+N_{SW}+N_{NE}+N_{SE}) \times\cos\theta+(T_{NE}+T_{SW}-T_{NW}-T_{SE})\sin\theta=2N_0, \tag{B5}$$

$$T_{NE}+T_{NW}+T_{SE}+T_{SW}-\frac{2I_M}{d^2}\dot{\Delta}=2T_0. \tag{B6}$$

It is now straightforward to write

$$\bar{B}_N(\theta)\begin{pmatrix}N_{NW}\\T_{NW}\\N_{NE}\\T_{NE}\end{pmatrix}+\bar{B}_S(\theta)\begin{pmatrix}N_{SW}\\T_{SW}\\N_{SE}\\T_{SE}\end{pmatrix} =\begin{pmatrix}2M\dot{u}_x\\2M\dot{u}_y\\\left(2M+\frac{2I_M}{d^2}\right)\dot{\Delta}\\\frac{2I_M}{d^2}\dot{\xi}\end{pmatrix}=2M\begin{pmatrix}\dot{u}_x\\\dot{u}_y\\(1+\kappa)\dot{\Delta}\\\kappa\dot{\xi}\end{pmatrix}, \tag{B7}$$

with

$$\bar{B}_N(\theta)=\begin{pmatrix}\cos\theta&-\sin\theta&-\cos\theta&-\sin\theta\\-\sin\theta&-\cos\theta&-\sin\theta&\cos\theta\\\sin\theta&1+\cos\theta&-\sin\theta&1+\cos\theta\\0&1&0&-1\end{pmatrix}, \tag{B8}$$

and

$$\bar{B}_S(\theta)=\begin{pmatrix}\cos\theta&\sin\theta&-\cos\theta&\sin\theta\\\sin\theta&-\cos\theta&\sin\theta&\cos\theta\\-\sin\theta&1+\cos\theta&\sin\theta&1+\cos\theta\\0&1&0&-1\end{pmatrix}, \tag{B9}$$

or

$$\begin{pmatrix}N_{NW}\\T_{NW}\\N_{NE}\\T_{NE}\end{pmatrix}=\bar{B}(\theta)\begin{pmatrix}N_{SW}\\T_{SW}\\N_{SE}\\T_{SE}\end{pmatrix}+2M\bar{C}(\theta)\begin{pmatrix}\dot{u}_x\\\dot{u}_y\\(1+\kappa)\dot{\Delta}\\\kappa\dot{\xi}\end{pmatrix}, \tag{B10}$$

with

$$\bar{B}(\theta)=-B_N^{-1}(\theta)B_S(\theta)=\begin{pmatrix}2\sin^2(\theta/2)&-\sin\theta&\cos\theta&-\sin\theta\\\sin\theta-\tan(\theta/2)&-\cos\theta&-\sin\theta+\tan(\theta/2)&2\sin^2(\theta/2)\\\cos\theta&\sin\theta&2\sin^2(\theta/2)&\sin\theta\\\sin\theta-\tan(\theta/2)&2\sin^2(\theta/2)&-\sin\theta+\tan(\theta/2)&-\cos\theta\end{pmatrix}, \tag{B11}$$

and

$$\bar{C}(\theta) = B_N^{-1}(\theta) = \frac{1}{2}\begin{pmatrix} 1 & -\csc\theta & \tan(\theta/2) & -\cot\theta \\ -\tan(\theta/2) & 0 & \dfrac{\cos\theta}{1+\cos\theta} & 1 \\ -1 & -\csc\theta & -\tan(\theta/2) & -\cot\theta \\ -\tan(\theta/2) & 0 & \dfrac{\cos\theta}{1+\cos\theta} & -1 \end{pmatrix}, \tag{B12}$$

and $\kappa = I_M/Md^2$.

[1] A. N. Schofield and C. P. Wroth, *Critical State Soil Mechanics* (McGraw-Hill, New York, 1968).

[2] C. K. K. Lun and S. B. Savage, ASME J. Appl. Mech. **54**, 47 (1987).

[3] V. Kumaran, J. Fluid Mech. **599**, 121 (2008) and references therein.

[4] D. Ertaş and T. C. Halsey, Europhys. Lett. **60**, 931 (2002); T. C. Halsey and D. Ertaş, e-print arXiv:cond-mat/0506170.

[5] J. T. Jenkins, Phys. Fluids **18**, 103307 (2006).

[6] GDR Midi, Eur. Phys. J. E **14**, 341 (2004).

[7] O. Baran, D. Ertas, T. C. Halsey, G. S. Grest, and J. B. Lechman, Phys. Rev. E **74**, 051302 (2006).

[8] O. Pouliquen, Phys. Fluids **11**, 542 (1999).

[9] L. E. Silbert, D. Ertaş, G. S. Grest, T. C. Halsey, D. Levine, and S. J. Plimpton, Phys. Rev. E **64**, 051302 (2001).

[10] S. F. Edwards, Physica A **249**, 226 (1998); S. Alexander, Phys. Rep. **296**, 65 (1998).

[11] The criterion that a contact be sliding reduces the number of kinematical constraints, but introduces an equivalent number of Coulomb constraints linking T to N, as in T. C. Halsey and D. Ertaş, Phys. Rev. Lett. **83**, 5007 (1999).

[12] Another source of dissipation is rolling friction, the dissipation that takes place at a rolling contact if the coefficient of friction is finite. This is a small effect, which is typically neglected in numerical studies. See K. L. Johnson, *Contact Mechanics* (Cambridge University Press, Cambridge, 1985), p. 306.

[13] Note that a similar argument could be used for a molecular fluid, in which case it would clearly be wrong, by equipartition—highlighting the importance of correlations.

[14] A similar approach, also based on frustration, was used by Ball and Blumenfeld to approach static states and perturbations thereof in R. C. Ball and R. Blumenfeld, Phys. Rev. Lett. **88**, 115505 (2002); R. Blumenfeld, Physica A **336**, 361 (2004).

[15] M. Weigel and D. Johnston, Phys. Rev. B **76**, 054408 (2007); for a review see R. Moessner, Can. J. Phys. **79**, 1283 (2001).

[16] R. Mahmoodi Baram, H. J. Herrmann, and N. Rivier, Phys. Rev. Lett. **92**, 044301 (2004); R. Mahmoodi Baram and H. J. Herrmann, *ibid.* **95**, 224303 (2005).

[17] F. Alonso-Marroquín, I. Vardoulakis, H. J. Herrmann, D. Weatherley, and P. Mora, Phys. Rev. E **74**, 031306 (2006).

[18] N. Rivier and D. M. Duffy, J. Phys. C **15**, 2867 (1982).